Deep-Water Fan Hierarchy: Assumptions, Evidence, and Numerical Modelling Analysis

Ibrahim Tinni Tahiru, Peter M. Burgess and Christopher Stevenson

Department of Earth, Oceans and Ecological Science, University of Liverpool.

ABSTRACT

Submarine fan strata are commonly described and interpreted assuming a nested, hierarchical organisation of elements, from beds, to lobe elements, lobes and lobe complexes. However, describing outcrop and subsurface strata following a particular conceptual method or model is never evidence in itself that the model or method accurately reflects the true nature of the strata. To develop better understanding of and methods for robust hierarchy identification and measurement we developed two metrics, a clustering strength metric that measures how much clustering is present in the spatial distribution of beds on a submarine fan, and a hierarchy step metric that indicates how many clustered hierarchical elements are present in the bed spatial distribution. Both metrics are applied to two quantitative fan models. The first is a very simple geometric model with 10 realisations ranging from a perfectly clustered hierarchy to a indistinguishable-from-random arrangement of beds. The second model, Lobyte3D, is a reduced-complexity process model which uses a steepest descent flow routing algorithm, combined with a simple but physically reasonable representation of flow velocity, erosion, transport and deposition thresholds, to generate detailed 3D representations of submarine fan strata. Application of the cluster strength and hierarchy step metric to the simpler model demonstrates how the metrics usefully characterise how much order and hierarchy is present in the fan strata. Application to four Lobyte3D models with increasingly complex basin-floor topography shows no evidence for true hierarchy, despite clear self-organisation of the model strata into lobes, suggesting that either Lobyte3D is missing key as yet unidentified processes responsible for producing hierarchy, or that interpretations of hierarchy are not realistic.

INTRODUCTION

Submarine fans are among the largest sedimentary accumulations (William, 1970; Posamentier and Kolla, 2003; Talling *et al.*, 2012) and serve as an essential record of Earth history, offering insights into both local and global geological processes (Emmel and Curray, 1984; Pirmez and Imran, 2003; Deptuck

et al., 2008; Picot *et al.*, 2016; Picot *et al.*, 2019; Rabouille *et al.*, 2017). Formed by a complex interplay of turbidity currents, other types of sediment mass flows, and various hydraulic processes, submarine fans are characterized by their complex stratigraphic architectures and depositional patterns (Straub and Pyles, 2012) Submarine fans are also often important reservoirs for the extraction of hydrocarbons and, increasingly importantly, for the sequestration of carbon (Pettingill, Weimer and Anonymous, 2002).

Understanding the organization of submarine fan strata is important for unravelling their formative processes and for deciphering the geological history they preserve. Previous studies have proposed hierarchical schemes to describe fan internal organization and characterise spatial and temporal variations in sedimentation patterns (Gardner, 2000; Pyles, 2008; Deptuck *et al.*, 2008; Prelat *et al.*, 2009; Prealat *et al.*, 2010) ; Mutti and Normak 1987; Gardner and Borer 2000, Pyles 2007; Deptuck et al. 2008, Prelat et al., 2009; Prelat et al., 2010). However, despite the significant progress made in characterizing submarine fan architecture, quantitative evidence to define hierarchy remains spares, and aspects of the fundamental mechanisms that would form hierarchical patterns remain poorly defined.

Existing Hierarchical Schemes

If submarine fans are hierarchical, they should show some form of systematic pattern of smaller-scale structures nested within and composing larger-scale structures. For example, in a hierarchical fan, fan lobes would be composed of lobe elements that are in turn each composed of many beds, each bed being one turbidite (Figure 1). Various examples of this type of hierarchical arrangement have been interpreted from outcrop, and subsurface data.

Deptuck et al. (2008) used ultra-high-resolution boomer seismic imagery with a vertical resolution of approximately 1 m to define a hierarchical classification for 20 lobes in a late Pleistocene submarine

fan offshore from East Corsica. The classification scheme defined four types of unit starting with a bed or bed-set deposited from single flows, with systematic lateral compensational offsets up to 500 m. Bed-sets stack to form lobe elements, which, in turn, stack to create composite lobes. Composite lobes are separated by disconformable surfaces, abrupt vertical shifts in acoustic facies, or the presence of thin drapes, all resulting from compensational stacking of lobe-elements with lateral offsets ranging from 500 to 2000 m triggered by local avulsion (Deptuck et al. 2008). Composite lobes fed by the same primary conduit stack to form lobe complexes, which frequently exhibit 3-5km lateral shifts between their thickest regions, interpreted to arise from large-scale channel-mouth avulsions. Abandoned composite lobes may be covered by several meters of hemipelagic drape, which may subsequently be eroded by later flows.

Based on well-exposed Permian deposits in the Tanqua depocenter of the Karoo Basin, South Africa Prelat et al. (2009) proposed a different four-fold hierarchical classification focused on the properties and geometry of fine-grained interlobe architectural units, which separate more sand-prone bodies. The lowest hierarchical level is single depositional event beds up to 0.5 m thick and hundreds of meters wide. Lobe elements up to 5m thick are composed of stacked beds and form the next higher hierarchical level. Genetically linked vertically stacked lobe elements, separated by fine-grained units typically less than 2 cm thick but occasionally up to 2m thick in topographic lows, create lobes up to 5 m thick with widths exceeding 20 km. Finally, lobe complexes are composed of stacked lobe bodies, up to 50 m thick and 40 km wide fed by a single upstream channel.

Macdonald *et al.*, (2011) focused on the process sedimentology and internal architecture of lobe deposits in the Carboniferous Ross Sandstone Formation, to propose a three-order hierarchy of bed-sets, lobe-elements, and composite lobes. Lobe-elements are formed by upward-thickening packages of bed-sets, often with basal mudstone units indicative of depositional shutdown. Mudstone thicknesses relate to the lateral distance and duration of avulsion separating compensationally-stacked lobe-elements.

(Cullis *et al.*, 2018) systematically reviewed and compared a representative selection of the most widely adopted deep-marine hierarchy schemes, to assess the principal characteristics of each hierarchical classification, the common diagnostic criteria used to attribute deposits to given hierarchical orders, and the causes of similarity and variability between different schemes. The review revealed recurrent observations underlying all the classification schemes, recommended that hierarchical relationships be categorised based on primary sedimentological observations, rather than through predefined schemes and concluded that a universal process-based hierarchy cannot be established. This is because of the difficulty in to reconcile the different hierarchical schemes arising partly from differences between the underlying studies such as the data types, scales of interest, specific environmental settings and in the significance given to the diagnostic criteria, as well as from the adoption of non-standard terminology.

Straub and Pyle (2012) used a modified version of the compensation index to test for statistically significant differences in compensation between different scales in hierarchically-classified strata. They also examined compensation variations between predominantly channelized and unchannelized submarine fan strata in each hierarchical class to test how compensation varies spatially. Their results suggest that hierarchical divisions based on compensation are justified, and that compensation increases along a longitudinal transect through distributive submarine fans.

Numerical Stratigraphic Forward Modelling as a Tool for Analysis of Submarine Fan Hierarchy

Numerical stratigraphic forward modelling has emerged as a useful tool for unravelling the complexities of sedimentary system (Paola, 2000; Burgess, 2013). By simulating the interplay between sediment transport, deposition, and erosion processes, these models provide valuable insights into the formation of stratigraphic patterns. Reduced-complexity models aim to capture the simplest possible set of processes that may be responsible for a specific stratigraphic pattern, while also

reducing computational cost, allowing multiple model runs and intensive analysis of model results, in this case to explore the emergence of hierarchical patterns within submarine fan systems.

This study utilizes the reduced-complexity stratigraphic forward model, Lobyte3D version 2.2, to investigate the hierarchical organization of submarine fan deposits. Lobyte3D is a three-dimensional reduced-complexity numerical stratigraphic forward model, developed to help understand how and why stacking patterns evolve in submarine fan depositional systems (Burgess *et al.*, 2019). Lobyte3D has been modified from its original form with new representations of key depositional processes, and most importantly, the addition of erosion as a function of flow velocity (Mackie et al., in review). In this paper Lobyte3D is used examine the architecture of submarine strata to to (1) access if there is any definite criteria to interpret lobes and (2) describe patterns present within each lobes. And (3) perform clustering analysis on the flow centroid to quantitatively identify and define lobes.

MODEL FORMULATION AND METHODOLOGY

Lobyte3D Formulation

Lobyte3D version 2.2 calculates turbidity flow routing, erosion and deposition, and the resulting stacking patterns that evolve as sediment accumulates on a submarine-fan surface. Transport and deposition are calculated on a simple orthogonal 50 by 50 km x-y grid with a cell edge dimension of 100m. Each model run consisted of 1000 flow events. Sediment enters the model at y0 at the top of a submarine slope. All the sediment volume in one flow event is moved downslope as one single depth-averaged packet of sediment in one model grid cell at each iteration following a steepest gradient descent down the slope. Deposition starts in the cell where depth-averaged flow velocity into the lowest adjacent cell is equal to or less than a specified sediment threshold velocity. Flow velocity is calculated such that.

$$v_f = v_i + (a * \emptyset) \qquad (1)$$

where V_f is the flow velocity, V_i is the velocity of the flow at the previous time step, a is the flow acceleration and Ø is the flow acceleration proportion taken to be 0.5

The flow acceleration a is given by.

$$a = v_m - v_i \qquad (2)$$

and the maximum velocity V_m converts shear velocity into whole flow velocity as a function of topographic gradient and is given by

$$v_m = \frac{v_s}{\sqrt{\sigma}} \qquad (3)$$

where V_s is the maximum shear velocity and σ is the basal friction coefficient.

Flow erosion rate is calculated as

$$\varepsilon_r = v_{se} * \frac{a}{b} \qquad (4)$$

where v_{se} is the settling velocity and a and b can are calculated as

$$a = C_e * Z^5 \qquad (5)$$

$$b = 1 + \frac{C_e}{0.3} * Z^5 \qquad (6)$$

where C_e is the erosion rate constant, and Z is the tractive stress which is calculated as follows.

$$Z = Re^6 * \frac{v_s}{v_{se}} \qquad (7)$$

where R_e is the particle Reynold number.

Four scenarios of Lobyte3D with varying degrees of complexity in the initial topography was used to model 1000 flow events. They include concave flat floor with no noise, very smoothed noise, smoothed noise, and raw noise. Each flow interrupts background hemipelagic deposition occurring at a rate of 0.02 m ky^{-1}. A flow repeat time of 1000 years will be maintained through each model run

representing a 1 M_y of flow history and deposition. Input parameters for the model include the initial topography, distribution of the grain-size, deposition threshold velocity to commence dispersive flow and deposition, concentration of the sediment, total volume of sediment transported by the flows (Table1).

For each model run, model behaviour was analysed by plotting each down-slope flow route and area of deposition in map view. Avulsion points were identified when the apex of flow deposition shifted substantially from the location of the apex of the previous flow.

Table 1: Lobyte3D input parameters

S/N	Parameter	Value
1	Hemipelagic deposition rate, per time step, m My^{-1}	0.02
2	Diffusion coefficient, m2 per My.	0.0
3	Density (kg/m^3) of the ambient fluid	1.00
4	Erosion rate constant (m/s)	1.3×10^{-10}
5	Basal friction coefficient	0.004
6	D50 (m) median grain diameter (medium/fine sand)	0.00025
7	Grain density in kg/m3 siliciclastic quartz/feldspar	2660
8	Depositional velocity threshold (m/s) to commence dispersive flow and deposition	0.1
9	Flow acceleration/deceleration coefficient	0.5
10	Total flow thickness, fluid and sediment mix (m)	100
11	Flow COG proportion	0.10

12	Volumetric sediment concentration	0.01
13	Minimum flow thickness (m)	0.001
14	Proportion of the height of ponding topographic lows to fill when flow is trapped	1.00
15	Flow Radiation Factor	2.0
16	Number of fractions in the depositional fraction profile	13

159

160 **Clustering Analysis and Hierarchy Metrics**

161 Clustering analysis is a numerical technique to classify data, originally developed as a natural sciences
162 method to make taxonomy more objective. (Everitt *et al.*, 2011), but now widely applied in earth
163 sciences (Simpson, Thatcher and Savage, 2012; Takahashi *et al.*, 2019) to identify patterns, group
164 similar objects, and uncover underlying structures within data. Cluster analysis partitions data based
165 on their similarities or dissimilarities, and often provides valuable insights into the organization and
166 relationships within the data (Everitt *et al.*, 2011). Clustering, unlike other classification techniques,
167 does not rely on preset classes and class-labelled samples, so is a relatively more objective method
168 (Jiawei Han, 2011).

169 Data point separation distances, or dissimilarity, are a fundamental aspect of many clustering
170 analyses, quantified using a wide range of dissimilarity measures (Gower and Legendre, 1986), often
171 in matrix form. Dissimilarity matrices capture pairwise dissimilarities, the distances between individual
172 data points, such that

173
$$D = \begin{bmatrix} 0 & & & & \\ d(2,1) & 0 & & & \\ d(3,1) & d(3,2) & 0 & & \\ \vdots & \vdots & \vdots & & \\ d(n,1) & d(n,2) & \cdots & \cdots & 0 \end{bmatrix}$$

Where $d(i,j)$ is the measured dissimilarity between objects i and j. since $d(i,j) = d(j,1)$, and $d(i,i) = 0$. Analysis of a dissimilarity matrix allows distinction between randomly distributed data where a broad spread of dissimilarity distances is expected, and clustered data, where the distances have a narrower range of values reflecting the specific distances within and between clusters; in clustered data, many of the dissimilarity distances are relatively small because many points occur in close proximity within the clusters.

Here we use a metric termed clustering strength to distinguish between clustered *xyz* data, and a randomly distributed set of *xyz* points. Clustering strength is calculated from the centroid separation distances such that

$$CSI = \left(\sum_{i=1}^{N} I(d_i \leq T)\right) \Big/ N$$

where *N* is the number of bed centroids, d_i is the separation distance between centroid point i and another centroid, *T* is a threshold distance, and *I* is an indicator function that returns 1 if or 0, depending the logical condition $d_i \leq T$. For a threshold distance that is 1% of the maximum dissimilarity distance in the system, values of clustering strength will approach zero as the degree of randomness in *xyz* points increase, and the value will always be higher for clustered data.

Once a degree of non-random clustering has been identified, the nature of the clustering can be assessed, specifically whether there is any hierarchical element such that smaller clusters themselves cluster to form larger clusters, and so on (e.g. Figure 1). Hierarchical Agglomerative Clustering Analysis (Gordon, 1987) is a bottom-up clustering analysis approach that starts with individual data points, merging them into new clusters based on their dissimilarity values, until all points are within one cluster. Euclidean dissimilarity distances were used because these most effectively measure bed centroid spatial relationships in xyz coordinate space, and the complete linkage method was selected because it has low sensitivity to outliers, and is relatively robust in noisy data (Jiawei Han, 2011), so a good choice to identify hierarchy levels.

198 Hierarchical cluster analysis results are plotted as a dendrogram, with cluster separation distance on
199 the Y-axis, and cluster number on the x-axis. The actual degree of hierarchy present in the dendrogram
200 can be assessed quantitatively by extracting dissimilarity distances between dendrogram bifurcation
201 points, and analysing these for clustering also; a hierarchical example should show clustering in these
202 bifurcation distances, because bifurcations should occur at specific scales reflecting the size and
203 separation distance of the various hierarchical elements. The hierarchy step metric is then the number
204 of distinct clusters identified in the dendogram bifurcation point distances, typically 1 for
205 indistinguishable from random points with little or no clustering, and otherwise a number
206 representing the number of hierarchical levels present in the data.

207

208 **RESULTS**

209 **Synthetic Lobe Model Results**

210 To provide a well-understood definitively hierarchical baseline for the analysis, eleven synthetic fan
211 lobe models were constructed and analysed, each comprising 1000 beds, with 40 beds in a lobe
212 element, five lobe elements per lobe, and five lobes in total. These models are range from perfectly
213 deterministic and hierarchical, with distinct lobes and lobe elements composed of beds arranged in a
214 simple retrogradational stacking pattern, to a completely stochastic example with a stochastic
215 distribution of bed centroids (Figure 2). The entirely deterministic fan arrangement follows the three
216 or four-fold hierarchy described in (Gervais *et al.*, 2006; Deptuck *et al.*, 2008; Prelat, Hodgson and
217 Flint, 2009) (Figure 1). A random offset is added to each x and y coordinate in the deterministic model,
218 and the magnitude of the added random element ranges from 0.05 to 0.5. For example, a model with
219 a random element of 0.2 has a random offset of each x and y coordinate ranging from -0.1 to 0.1.

220 For each synthetic fan lobe model, cluster strength was calculated, and also hierarchy step values were
221 derived from dendogram analysis (Figure 3). The cluster strength values range from a high of $5.7\times10^{-}$

222 ^{3} for the completely deterministic hierarchically clustered fan, to 1.0×10^{-5} for the entirely random bed
223 centroid points, and the decrease in the metric value is quite sharp as the magnitude of random point
224 offset increases (Figure 4A). The dendogram hierarchy analysis shows a similar pattern. The two least-
225 random-component models yield a hierarchy step value of 3, an accurate measurement of the number
226 of hierarchical levels built in to each model (Figure 4B). In contrast, the models with a random offset
227 value of 0.2 and greater have a hierarchy step value of 1 indicating that a random offset of 0.2 or more
228 is enough to remove any detectable hierarchy.

229

230 **Lobyte3D Model Results**

231 Lobyte3D was run with four different initial topographies defining scenarios with no noise, very
232 smoothed noise, smoothed noise, and raw noise. Strike-oriented cross-sections, 3D views of the
233 channel, bed and lobe stacking patterns, and bed centroid maps from these different initial
234 topographies are used to understand how variations in initial topography control avulsion, fan
235 stacking, and the hierarchical organization of the modelled submarine fan strata.

236 *Avulsion Cycle Processes*

237 The avulsion process is key to forming lobes and therefore key to generating any stratal hierarchy
238 present, so it is important to understand exactly how avulsion occurs in the model. Evolving flow
239 routing shows substantial changes during avulsion, bypassing previous mounded depositional
240 topography, and cutting a new section of channel that bypasses sediment further into the basin to the
241 point where the initial basin floor slope is low enough to decelerate the flow enough to trigger
242 deposition.

243 Analysis of the first avulsion in the no noise case reveals the detail of how avulsion occurs in Lobyte3D.
244 Prior to flow 190, deposition was backstepping up the basin-margin slope, partially backfilling the
245 mouth of the previously cut channel (Figure 5). Upslope backstepping occurred due to flow interaction

246 at the channel-lobe transition, with strata deposited from previous flows triggering flow deceleration
247 and further deposition. As strata backstep upslope, depositional relief at the channel mouth on the
248 proximal mound edge increased, and magnitude of deceleration when flows reach this depositional
249 topography also increased. Each time a flow encounters a mound that has been built by previous
250 flows, the flow will continue to follow the steepest available down-slope route, and therefore tend to
251 divert left or right to climb over the lowest-relief part of the mound. Flow velocity prior to climbing
252 the depositional mound tends to increase through time as deposition backsteps up the basin-margin
253 slope, and by flow 190, the flow had sufficient remaining velocity after climbing the depositional
254 mound (Figure 5) to continue to flow, accelerate down from the crest of the mound, and start to cut
255 a new channel. Flow routing through the new channel bypasses the positive topography produced by
256 the previous lobe deposition, defines a new route further into the basin (Figure 5b), and starts to
257 deposit a new lobe, defining an avulsion event.

258 Rather obviously this is a much-simplified representation of what actually happens in deep-water
259 depositional systems. For instance, several processes have been investigated to produce instability
260 that results in avulsion-threshold circumstances. Channel sinuosity, channel lengthening, channel
261 thalweg and levee aggradation, and channel-relief reduction are some of these causes (Kolla, 2007;
262 Prelat, Hodgson and Flint, 2009; Groenenberg *et al.*, 2010). In this analysis we assume that this
263 modelled avulsion process is sufficiently realistic and representative enough of the real physical
264 process to form the basis for at least initial numerical experiment exploration of how this behaviour
265 influences fan lobe geometry stacking and potential hierarchy.

266

267 *Flow Routing and Stacking Patterns*

268 All four modelled scenarios generated a multi-km-scale submarine fan (Figure 7) consisting of
269 interbedded turbidite event beds and background hemipelagic strata organised as more-or-less
270 discrete lobes (Figure 8) broadly comparable to typical observed submarine-fan bathymetry and

successions (Romans *et al.*, 2009; Romans *et al.*, 2011; Prelat, Hodgson and Flint, 2009; Prelat and Hodgson, 2013). The no noise initial topography produces the most systematic lobe stacking with a simple compensational stacking pattern and lobe boundaries clearly defined by a few meters of hemipelagic sediments (Figure 8A). Each lobe is composed of around 60-to-200 mostly contiguous, spatially-clustered backstepping flow events. Lobes have a simple stacking pattern, separated by progressive lateral 1-2km shift in focus of deposition, and a mean duration of 114 ky (Figure 8A).

The very smooth noise initial topography produces similar but slightly more complex lobe stacking pattern (Figure 8B). These lobes consist of around 50 to 130 aggradational and backstepping beds with a lateral lobe separation distance of 2-4 km and a mean duration of 83 ky (Figure 8B, Figure 9B). The smooth noise initial topography case still shows some discrete lobes, but lobe structure and stacking are more complex (Figure 7C). Where distinct enough to measure, lobes consist of 35-70 contiguous spatially clustered flow events, with lateral lobe separation distance ranging from 0.5 to 2 km and a mean duration of 50 ky (Figure 8C, Figure 9C). Finally, the raw noise initial topography shows the most complex lobe stacking pattern lacking any clear trend (Figure 7D, Figure 9D). These lobes are even more difficult to define. Where discrete enough to define, lobes consist of 5 to 270 aggradational and backstepping stacked beds with a separation distance of 1 to 3 km, but also the highest gradual lateral shift within each lobe (Figure 8D) and a mean duration of 112 ky.

Quantification of Clustering and Hierarchy in Lobyte3D Results

Cluster strength values for the four Lobyte3D models range from 2.51×10^{-3} to 1.14×10^{-3} (Figure 4A) and the smoothed noise initial topography generates the highest clustering strength, suggesting that smoothed noise in the basin-floor topography can enhance clustering relative to the case with the simplest no-noise topography. In contrast, the raw noise basin-floor topography model has the lowest clustering strength (Figure 4A) due to the irregular topography disrupting the regular stacking and avulsion pattern required for clustering. All four model runs generate strata with a hierarchical step

296 value of 1, indicating that no hierarchy is detectable in the spatial distribution of bed centroids, despite
297 the clustering. This suggests that although the clustering produces clear lobe structures, particularly
298 in the no noise and smoothed noise cases, this bed-lobe distinction is not enough to define a hierarchy
299 measured by this dendogram-derived metric.

300

301 # DISCUSSION

302 **Reduced complexity models**

303 Reduced complexity models are, by design, very much simplified representations of the complex
304 processes that generate real strata (Liang et al., 2015). Consequently, results from reduced complexity
305 models must be used carefully, and not over interpreted or assumed to have predictive power beyond
306 what is reasonably supported by their constituent process representations. However, these models
307 also have some substantial advantages over more complex models, particularly their lower
308 computational cost, and perhaps most importantly, the fact that if a reduced complexity model
309 demonstrates a particular emergent behaviour, the process representation in the model is quite likely
310 to be the simplest possible representation of that process.

311 In this case Lobyte3D shows avulsion events that divert deposition into new locations clustering sets
312 of beds to form lobes. Critical elements in the model necessary for this a steepest-descent transport
313 algorithm and a gradient threshold for initiation for turbidite bed deposition. Both these elements are
314 represented in a very simple but physically reasonable way, and do seem to operate to some degree
315 in real submarine fan systems. Given this the resulting lobe formation in the model is probably realistic
316 enough to offer some basic but useful insight in deep-water fan processes and structure. However, it
317 is also important to remember that additional and more realistic representations of key processes, for
318 example more detail in the 3D structure and spatial distribution of each flow and consideration of a
319 range of grain sizes in each flow may generate different avulsion process and different fan structures

(e.g. (Wahab *et al.*, 2022)) and (Hamilton, Strom and Hoyal, 2015) found that uneven topography increases channel avulsion likelihood due to localized variations in sediment concentration, leading to mouth bar formation and hydraulic jumps. Clearly these processes and controls require further investigation with more complex models, but starting with the simplest model seems sensible.

Influence of initial topography

Lobyte3D models in this analysis show substantial influence of initial topography on flow routing, avulsion, and lobe stacking patterns. Previous studies have shown or interpreted a similar influence of topography in shaping submarine fan evolution and architecture (Groenenberg *et al.*, 2010; Straub and Pyles, 2012; Hamilton, Strom and Hoyal, 2015; Cullis *et al.*, 2018; Ferguson *et al.*, 2020); taken together these results support the hypothesis that initial topography influences lobe switching and avulsion timing (Piper and Normark, 2001; Gervais *et al.*, 2006; Groenenberg *et al.*, 2010; Ferguson *et al.*, 2020). However, the formulation of Lobyte3D is perhaps particularly sensitive to small changes in seafloor topography, especially in terms of flow routing prior to deposition, so further work developing more complex model formulations or testing this effect with other numerical and analogue models is required.

Absence of hierarchy

There is no hierarchy present in these Lobyte3D results; all modelled strata show detectable non-random clustering, as indicated by comparison with the entirely synthetic fan models, but all the Lobyte3D models have a hierarchical step value 1. This combination of cluster and hierarchy metric values indicate that no hierarchy is detectable in the spatial distribution of bed centroids, despite the clustering.

Clearly absence of a hierarchy in strata calculated in a reduced complexity numerical model is not necessarily evidence that hierarchy does not occur in real deep-water fan strata. However, nor is interpretation of outcrop and subsurface data following a conceptual model of stratal hierarchy evidence that the deep-water fan strata really are hierarchical. Failure to reproduce hierarchy in a very simple numerical model highlights two end-member possibilities; either hierarchy is a real feature of deep-water fan strata, but occurs by processes not adequately represented in Lobyte3D, or the interpretations of hierarchy in outcrop and subsurface strata are an over-interpretation of limited data with insufficient quantitative evidence to be properly robust.

Avulsion is a key control on hierarchy formation because it is the main process forming clustered entities such as lobes. Avulsion in Lobyte3D happens in a simplified and specific way that likely does not capture the range of different and perhaps more complex mechanisms that operate in real submarine fan systems (Hamilton *et al*., 2015; Ortiz-Karpf *et al.*, 2015; Qi *et al.*, 2022; de Haas *et al.*, 2016). Clearly therefore further modelling and model development is required, with Lobyte3D or other process models including analogue models perhaps, to explore how other avulsion processes might behave differently and produce hierarchical clustering.

Until now, interpretations of hierarchy in submarine fan strata have been mostly qualitative, and this lack of quantitative evidence does mean that conclusions of hierarchy are much more tenuous than has perhaps been recognised. More quantitative analysis is therefore required, but a key challenge is how to analyse limited data, for example one-dimensional vertical sections, to provide metrics that can reliably identify and present or absence of hierarchy developed in three-dimensional strata; most current interpretations do not recognise or account for this uncertainty (Gervais et al. 2006; Deptuck et al. 2008; Prelat et al. 2009; MacDonald et al. 2011), suggesting that hierarchical patterns observed in previous studies are probably not universally applicable to all submarine fan systems (Cullis et al. 2018; Ferguson et al. 2020), and development of further tools for quantification of hierarchy with limited outcrop and subsurface data is essential.

CONCLUSIONS

1. Submarine fan strata are commonly described and interpreted to have a nested, hierarchical organisation of elements, but quantitative evidence from outcrop and subsurface data to support this interpretation is limited.
2. Two new metrics are defined, calculated and used to identify the degree of hierarchy present in the modelled fan strata. A clustering strength metric measures how much clustering is present in the spatial distribution of Lobyte3D beds, and a hierarchy step metric indicates how many clustered hierarchical elements are present in the bed spatial distribution.
3. Both metrics applied to a definitively hierarchical geometric fan model with ten progressively more randomised realisations, shows that the combined metrics can clearly distinguish between hierarchical and non-hierarchical realisations.
4. The combined metrics also show that there is no hierarchy present in the four Lobyte3D realisations, suggesting that either Lobyte3D is missing key as yet unidentified processes responsible for producing hierarchy, or that hierarchal interpretations of outcrop and subsurface data are more complicated and less realistic than typically assumed.

REFERENCES

Burgess, P. M. (2013) 'CarboCAT: A cellular automata model of heterogeneous carbonate strata', *Computers & geosciences,* 53, pp. 129-140.

Burgess, P. M., Masiero, I., Toby, S. C. and Duller, R. A. (2019) 'A big fan of signals? Exploring autogenic and allogenic process and product in a numerical stratigraphic forward model of submarine-fan development', *Journal of sedimentary research,* 89(1), pp. 1-12.

Cullis, S., Colombera, L., Patacci, M. and McCaffrey, W. D. (2018) 'Hierarchical classifications of the sedimentary architecture of deep-marine depositional systems', *Earth-science reviews,* 179, pp. 38-71.

de Haas, T., van den Berg, W., Braat, L., Kleinhans, M. G. and Mohrig, D. (2016) 'Autogenic avulsion, channelization and backfilling dynamics of debris flow fans', *Sedimentology,* 63(6), pp. 1596-1619.

Deptuck, M. E., Piper, D. J. W., Savoye, B. and Gervais, A. (2008) 'Dimensions and architecture of late Pleistocene submarine lobes off the northern margin of east Corsica', *Sedimentology,* 55(4), pp. 869-898.

Emmel, F. J. and Curray, J. R. (1984) 'The Bengal submarine fan, Northeastern Indian Ocean', *Geo-marine letters,* 3(2-4), pp. 119-124.

Everitt, B. S., Landau, S., Leese, M. and Stahl, D. (2011) *Cluster Analysis. Wiley series in probability and statistics* 5. Aufl. edn. Newark: Wiley.

Ferguson, R. A., Kane, I. A., Eggenhuisen, J. T., Pohl, F., Tilston, M., Spychala, Y. T. and Brunt, R. L. (2020) 'Entangled external and internal controls on submarine fan evolution: an experimental perspective', *The depositional record,* 6(3), pp. 605-624.

Gervais, A., Savoye, B., Mulder, T. and Gonthier, E. (2006) 'Sandy modern turbidite lobes; a new insight from high resolution seismic data', *Marine and petroleum geology,* 23(4), pp. 485-502.

Gordon, A. D. (1987) 'A Review of Hierarchical Classification', *Journal of the Royal Statistical Society. Series A. General,* 150(2), pp. 119-137.

Gower, J. C. and Legendre, P. (1986) 'Metric and Euclidean properties of dissimilarity coefficients', *Journal of classification,* 3(1), pp. 5-48.

Groenenberg, R. M., Hodgson, D. M., Prelat, A., Luthi, S. M. and Flint, S. S. (2010) 'Flow-deposit interaction in submarine lobes; insights from outcrop observations and realizations of a process-based numerical model', *Journal of sedimentary research,* 80(3), pp. 252-267.

Hamilton, P. B., Strom, K. B. and Hoyal, D. C. J. D. (2015) 'Hydraulic and sediment transport properties of autogenic avulsion cycles on submarine fans with supercritical distributaries', *Journal of geophysical research. Earth surface,* 120(7), pp. 1369-1389.

421 Jiawei Han, J. P. M. K. (2011) *Data Mining: Concepts and Techniques. The Morgan Kaufmann Series in*
422 *Data Management Systems* 2nd Edition edn.: Elsevier Science.
423 Kolla, V. (2007) 'A review of sinuous channel avulsion patterns in some major deep-sea fans and factors
424 controlling them', *Marine and petroleum geology,* 24(6-9), pp. 450-469.
425 Macdonald, H. A., Peakall, J., Wignall, P. B. and Best, J. (2011) 'Sedimentation in deep-sea lobe-
426 elements; implications for the origin of thickening-upward sequences', *Journal of the Geological*
427 *Society,* 168(2), pp. 319-332.
428 Michael H. Gardner, J. M. B. (2000) 'Abstract: Submarine channel architecture along a slope to basin
429 profile, Brushy Canyon Formation, West Texas', *AAPG bulletin,* 84 (2000).
430 Ortiz-Karpf, A., Hodgson, D. M. and McCaffrey, W. D. (2015) 'The role of mass-transport complexes in
431 controlling channel avulsion and the subsequent sediment dispersal patterns on an active margin: The
432 Magdalena Fan, offshore Colombia', *Marine and petroleum geology,* 64, pp. 58-75.
433 Paola, C. (2000) 'Quantitative models of sedimentary basin filling', *Sedimentology,* 47(s1), pp. 121-178.
434 Pettingill, H. S., Weimer, P. and Anonymous (2002) 'Worldwide deepwater exploration and
435 production; past, present, and future', *Leading edge (Tulsa, Okla.),* 21(4), pp. 371-376.
436 Picot, M., Droz, L., Marsset, T., Dennielou, B. and Bez, M. (2016) 'Controls on turbidite sedimentation;
437 insights from a quantitative approach of submarine channel and lobe architecture (late Quaternary
438 Congo Fan)', *Marine and petroleum geology,* 72, pp. 423-446.
439 Picot, M., Marsset, T., Droz, L., Dennielou, B., Baudin, F., Hermoso, M., de Rafelis, M., Sionneau, T.,
440 Cremer, M., Laurent, D. and Bez, M. (2019) 'Monsoon control on channel avulsions in the Late
441 Quaternary Congo Fan', *Quaternary science reviews,* 204, pp. 149-171.
442 Piper, D. J. W. and Normark, W. R. (2001) 'Sandy fans; from Amazon to Hueneme and beyond', *AAPG*
443 *bulletin,* 85(8), pp. 1407-1438.
444 Pirmez, C. and Imran, J. (2003) 'Reconstruction of turbidity currents in Amazon Channel', *Marine and*
445 *petroleum geology,* 20(6), pp. 823-849.
446 Posamentier, H. W. and Kolla, V. (2003) 'Seismic geomorphology and stratigraphy of depositional
447 elements in deep-water settings', *Journal of sedimentary research,* 73(3), pp. 367-388.
448 Prealat, A., Covault, J. A., Hodgson, D. M., Fildani, A. and Flint, S. S. (2010) 'Intrinsic controls on the
449 range of volumes, morphologies, and dimensions of submarine lobes', *Sedimentary geology,* 232(1-2),
450 pp. 66-76.
451 Prelat, A. and Hodgson, D. M. (2013) 'The full range of turbidite bed thickness patterns in submarine
452 lobes; controls and implications', *Journal of the Geological Society,* 170(1), pp. 209-214.

Prelat, A., Hodgson, D. M. and Flint, S. S. (2009) 'Evolution, architecture and hierarchy of distributary deep-water deposits; a high-resolution outcrop investigation from the Permian Karoo Basin, South Africa', *Sedimentology,* 56(7), pp. 2132-2154.

Pyles, D. R. (2008) 'Multiscale stratigraphic analysis of a structurally confined submarine fan; Carboniferous Ross Sandstone, Ireland', *AAPG bulletin,* 92(5), pp. 557-587.

Qi, K., Gong, C., Steel, R. J., Shao, D., Ding, L. and Ma, H. (2022) 'The formation and development of avulsions and splays of submarine channel systems: Insights from 3D seismic data from the northeastern Bengal Fan', *Sedimentary geology,* 440, pp. 106239.

Rabouille, C., Baudin, F., Dennielou, B. and Olu, K. (2017) 'Organic carbon transfer and ecosystem functioning in the terminal lobes of the Congo deep-sea fan: outcomes of the Congolobe project', *Deep-sea research. Part II, Topical studies in oceanography,* 142(2), pp. 1-6.

Romans, B. W., Fildani, A., Hubbard, S. M., Covault, J. A., Fosdick, J. C. and Graham, S. A. (2011) 'Evolution of deep-water stratigraphic architecture, Magallanes Basin, Chile', *Marine and petroleum geology,* 28(3), pp. 612-628.

Romans, B. W., Normark, W. R., McGann, M. M., Covault, J. A. and Graham, S. A. (2009) 'Coarse-grained sediment delivery and distribution in the Holocene Santa Monica Basin, California; implications for evaluating source-to-sink flux at millennial time scales', *Geological Society of America bulletin,* 121(9-10), pp. 1394-1408.

Simpson, R. W., Thatcher, W. and Savage, J. C. (2012) 'Using cluster analysis to organize and explore regional GPS velocities', *Geophysical research letters,* 39(18), pp. n/a.

Straub, K. M. and Pyles, D. R. (2012) 'Quantifying the hierarchical organization of compensation in submarine fans using surface statistics', *Journal of sedimentary research,* 82(11), pp. 889-898.

Takahashi, A., Hashimoto, M., Hu, J. C., Takeuchi, K., Tsai, M. C. and Fukahata, Y. (2019) 'Hierarchical Cluster Analysis of Dense GPS Data and Examination of the Nature of the Clusters Associated With Regional Tectonics in Taiwan', *Journal of geophysical research. Solid earth,* 124(5), pp. 5174-5191.

Talling, P. J., Masson, D. G., Sumner, E. J. and Malgesini, G. (2012) 'Subaqueous sediment density flows: Depositional processes and deposit types', *Sedimentology,* 59(7), pp. 1937-2003.

Wahab, A., Hoyal, D. C., Shringarpure, M. and Straub, K. M. (2022) 'A dimensionless framework for predicting submarine fan morphology', *Nature communications,* 13(1), pp. 7563-7563.

William, R. N. (1970) 'Growth Patterns of Deep-Sea Fans', *AAPG bulletin,* 54.

Figure captions

Figure 1: An idealised model of hierarchical stacking patterns with three primary clusters each defining a lobe, and each further subdivided into four lobe-element sub-clusters, each of which is composed of a series of individual turbidite beds.

Figure 2: Centroid plot of synthetic fan models, with a normalised 0-to-1 *xy* coordinate range, and varying degrees of randomness in the bed centroid *xy* coordinates A. Totally deterministic and hierarchical, without random offset, B. moderate randomness with a random element of 0.1, C. significant randomness with a random element of 0.5. D. Totally random model with a random element of 1.0. As randomness increases from 0 to 1, the distinction between clusters diminishes, reflecting a transition from well-defined, hierarchical patterns, to a random arrangement of beds.

Figure 3. Dendograms calculated from a selection of synthetic fan scenarios. A. Totally deterministic and hierarchical model. B. Synthetic model with a random offset of 0.2. C. Synthetic model with a random offset of 0.5. D. Totally stochastic model with a random offset

Figure 4. Measurements of clustering and hierarchy in the synthetic fan models. A. Cluster strength plotted against the maximum random point separation shows that cluster strength decreases sharply from a maximum with no random element in the synthetic fan model, to much lower values for a maximum random offset of 0.1 and greater. B. The hierarchy step metric shows 3 hierarchical levels for maximum random offsets less than 0.1, and only one level, so no evidence of hierarchy, for greater levels of randomness in the synthetic fan models.

Figure 5. Topography from the no noise model showing the lobe (yellow), channel, and sediment flow paths (blue) for pre-avulsion flow 189 (a) and post-avulsion flow 190 (b) at the avulsion node location. Yellow cells indicate the location of deposition of the previous flow. Flow 189 deposits a small part of its sediment load at the channel mouth, diverts and climbs over previously-deposited topography, and decelerates and deposits. Flow 190, in contrast, deposits, ascends, but retains enough velocity to divert, accelerate, and start cutting a new channel, defining a new route to begin to deposit a new lobe.

Figure 6. Plot of the no-noise model topography (solid lines) and flow velocity (dashed lines) versus flow distance along the route of flows 189 (red lines) and 190 (blue lines). Prior to avulsion, flow 189 velocity first reverses sign as it hits an opposite-facing slope on previous depositional mound topography, deposits some sediment in the channel mouth that accretes to the back of the previous depositional mound, then decelerates to near zero velocity climbing the prior topography, below the threshold velocity for continued transport, at which point full flow deposition commences. In contrast, flow 190 has sufficient velocity on the slightly steeper slope such that flow deceleration climbing the mound is insufficient to trigger deposition, leaving sufficient remaining velocity to flow over the mound crest, accelerate down the mound lee slope, and start cutting a new channel that defines a new avulsed route further into the basin.

Figure 7. 3D views for each of the different initial topographies, showing how successive flows in different colours backstep up-slope to form lobes, and then avulse as flows divert around the depositional topography created by previous flows using different initial topography. A. no noise topography, B. very smooth noise, C. smooth noise, and D. raw noise topography. Blue circles show the apex position of each turbidite bed, so show stacking pattern of beds, which is mostly aggradational with a slight retrogradational element.

Figure 8. Strike-oriented cross-section and chronostratigraphic plot a y = 15km, for each of the four initial topographies, showing distinct packages of flow deposits each separated by a hemipelagic unit. A. no noise topography, B. very smooth noise, C. smooth noise, and D. raw noise. Clustering of beds is

evident in all four model runs, but becomes more complex as the degree of smoothing of the noise in the initial topography is reduced. Note different colours in the cross section delineate turbidite beds, and tringle geometries are backfilled channels, and in the chronostratigraphic diagram light blue indicates lobe deposition while pale pink indicates channel erosion.

Figure 9. Plot of centroids of stacked beds obtained from Lobyte3D with different initial topographies. A: No noise, 3 lobes. b: very smooth noise, 4 lobes. c: smooth noise, 4 – 5 lobes. d: raw noise, 6 lobes. This figure illustrates the impact of four different initial topographies. The plot unveils a distinct pattern in the flow behaviour, characterized by backstepping of flows followed by avulsion events, leading to the deposition of sediment in new locations. Each bar on the plot represents the chronological order of flow deposits, ranging from the earliest to the latest. The visualization provides valuable insights into the dynamic nature of sedimentation processes and the influence of different initial topographies on the stacking patterns of beds.

Figure 10. Measurements of clustering and hierarchy in the four Lobyte3D models, plotted on top of the synthetic fan model values. Note that Lobyte3D data points are plotted at the point on the x-axis where, according to simple linear interpolation, the synthetic fan model would have the same cluster strength value, assuming that the cluster strength is a reasonable measure of the degree of randomness present in the bed centroid *xy* distribution. See text for discussion.

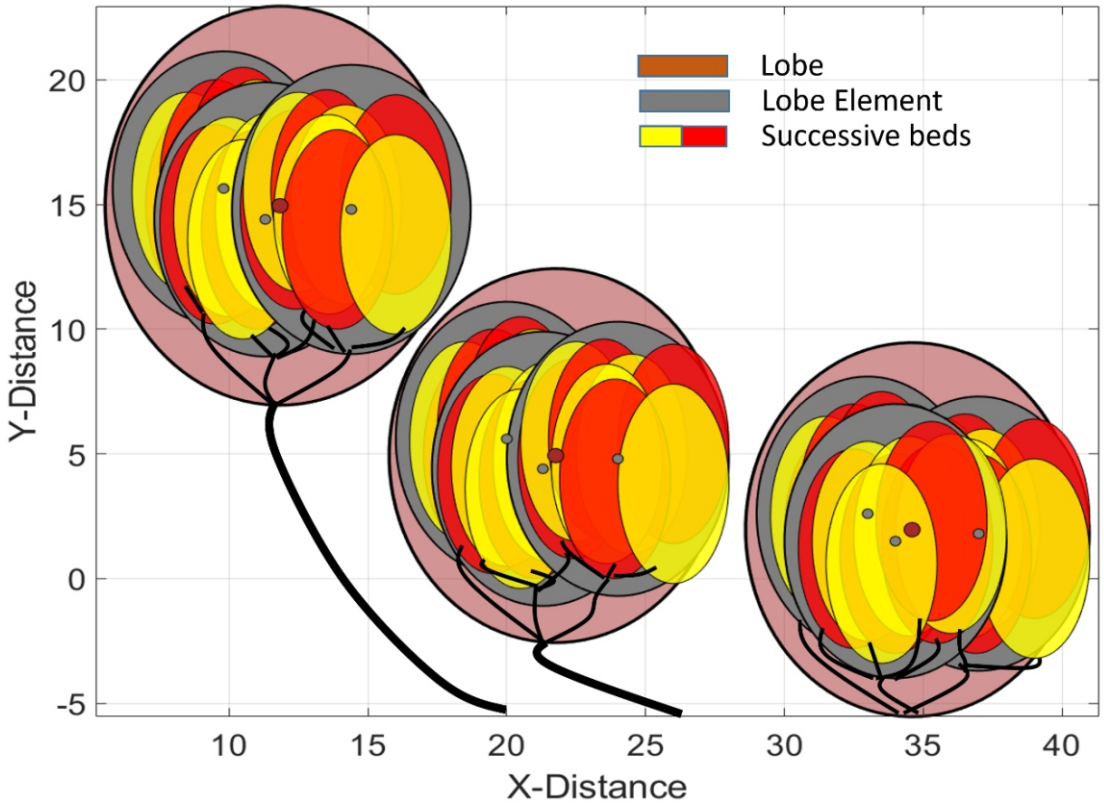

Figure 1

Figure

Click here to access/download;Figure;Figure 2 synthetic fan models.pdf

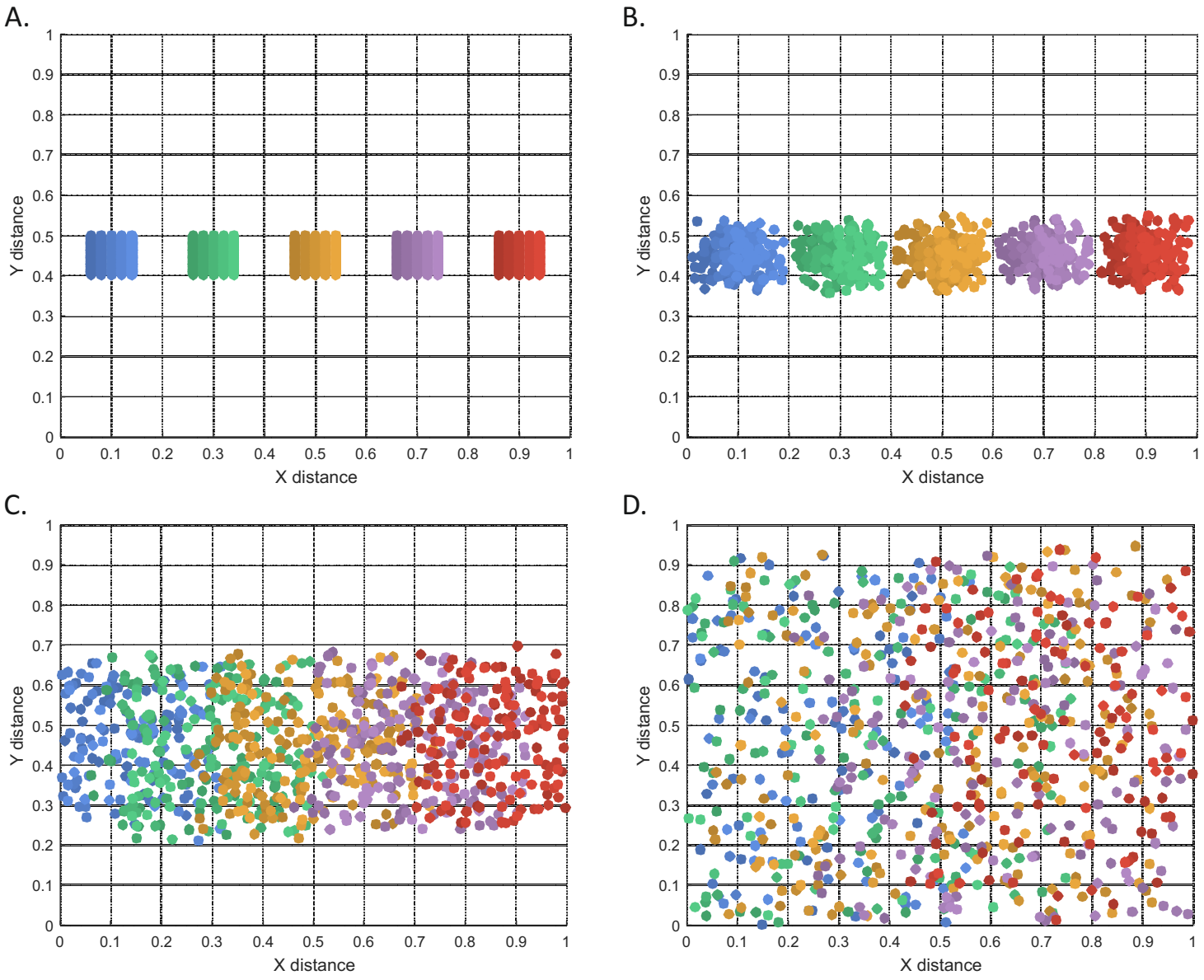

Figure

Click here to access/download;Figure;Figure 3 dendograms synthetic fan model.pdf

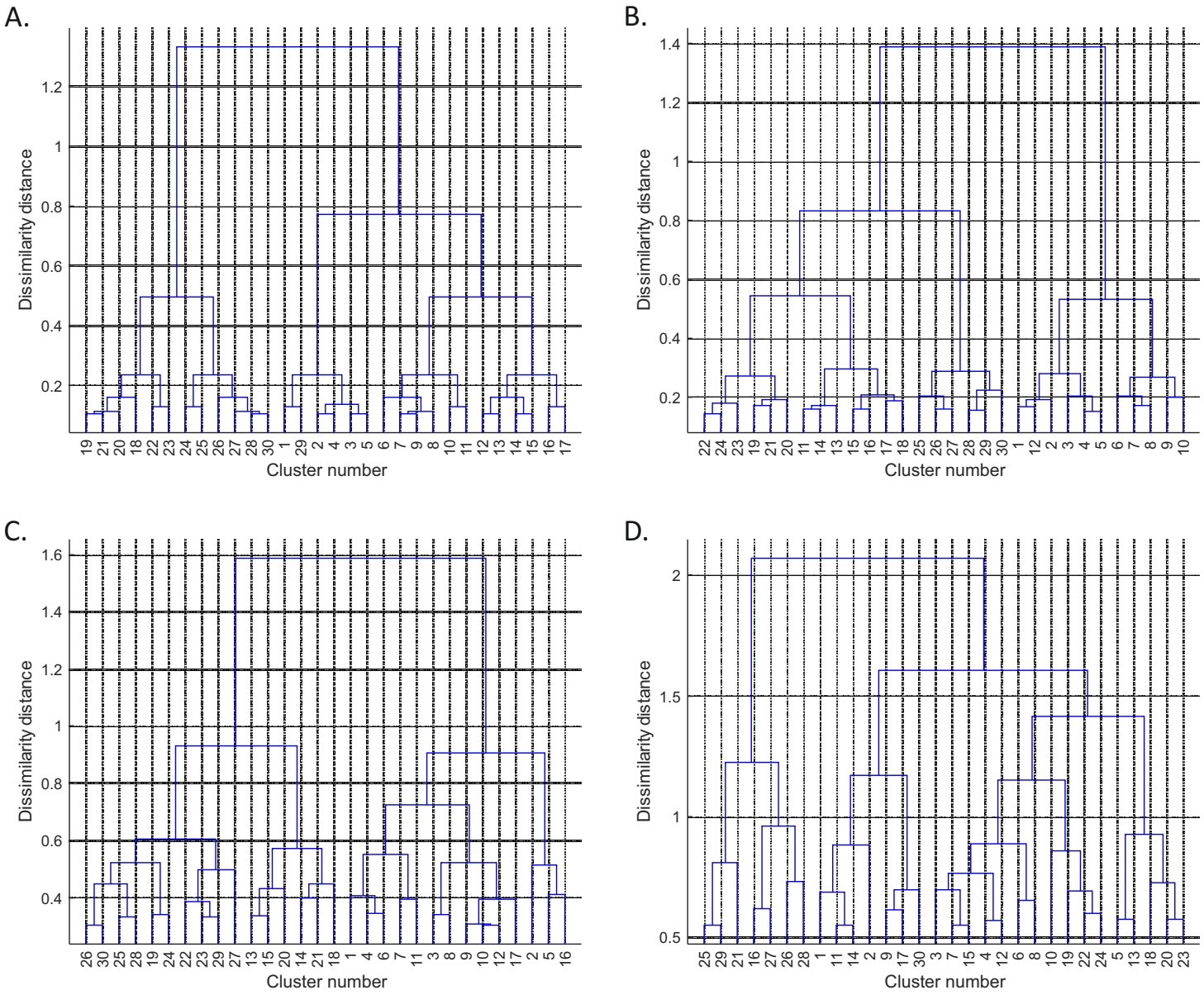

Figure

Click here to access/download;Figure;Figure 4 cluster and hiearchy metric plots.pdf

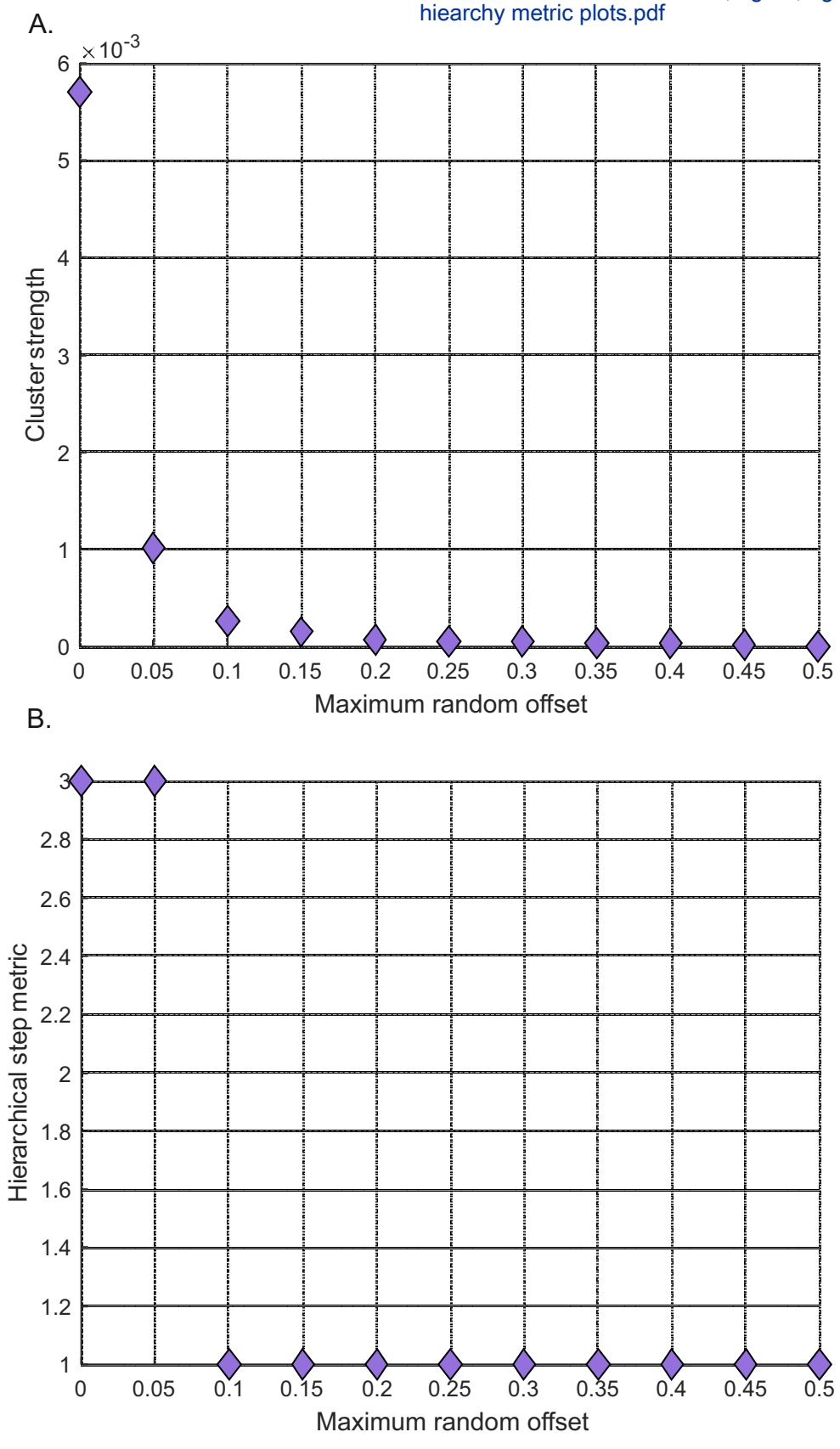

Figure

Click here to access/download;Figure;Figure 5 Avulsion Process.pdf

A.

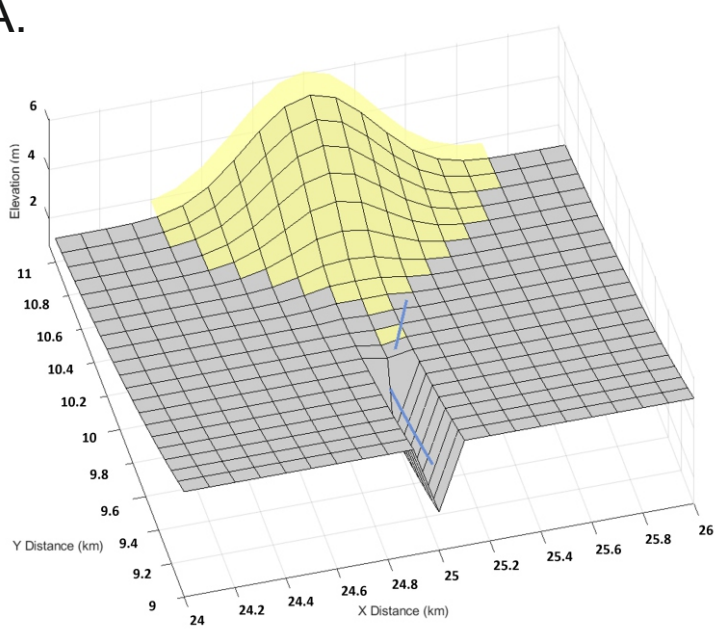

B.

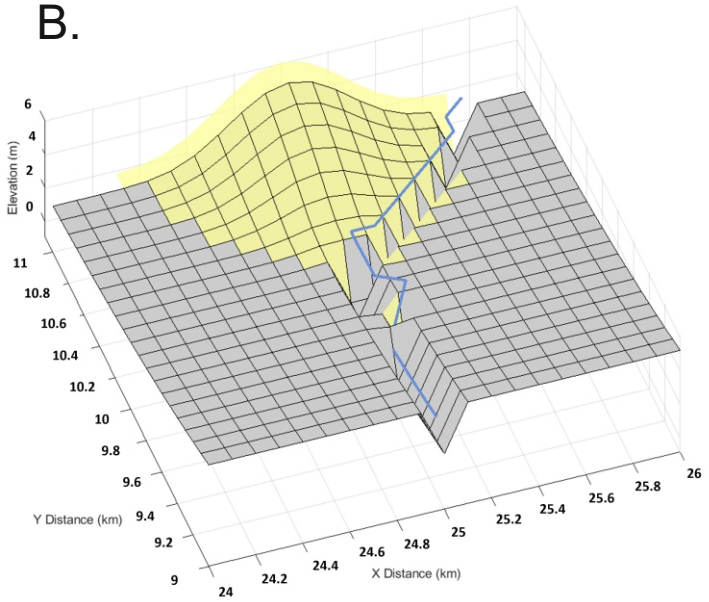

Figure

Click here to access/download;Figure;Figure 6 Flow Velocity Avulsion.pdf

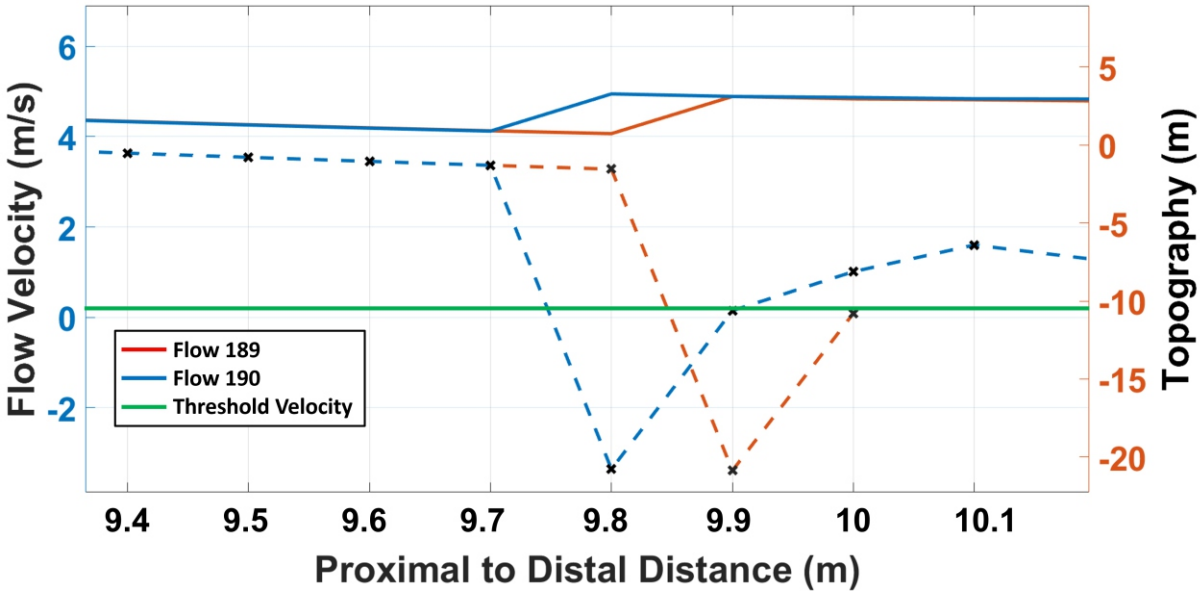

Figure

Click here to access/download;Figure;Figure 7 Lobyte3d strata 3D views.pdf

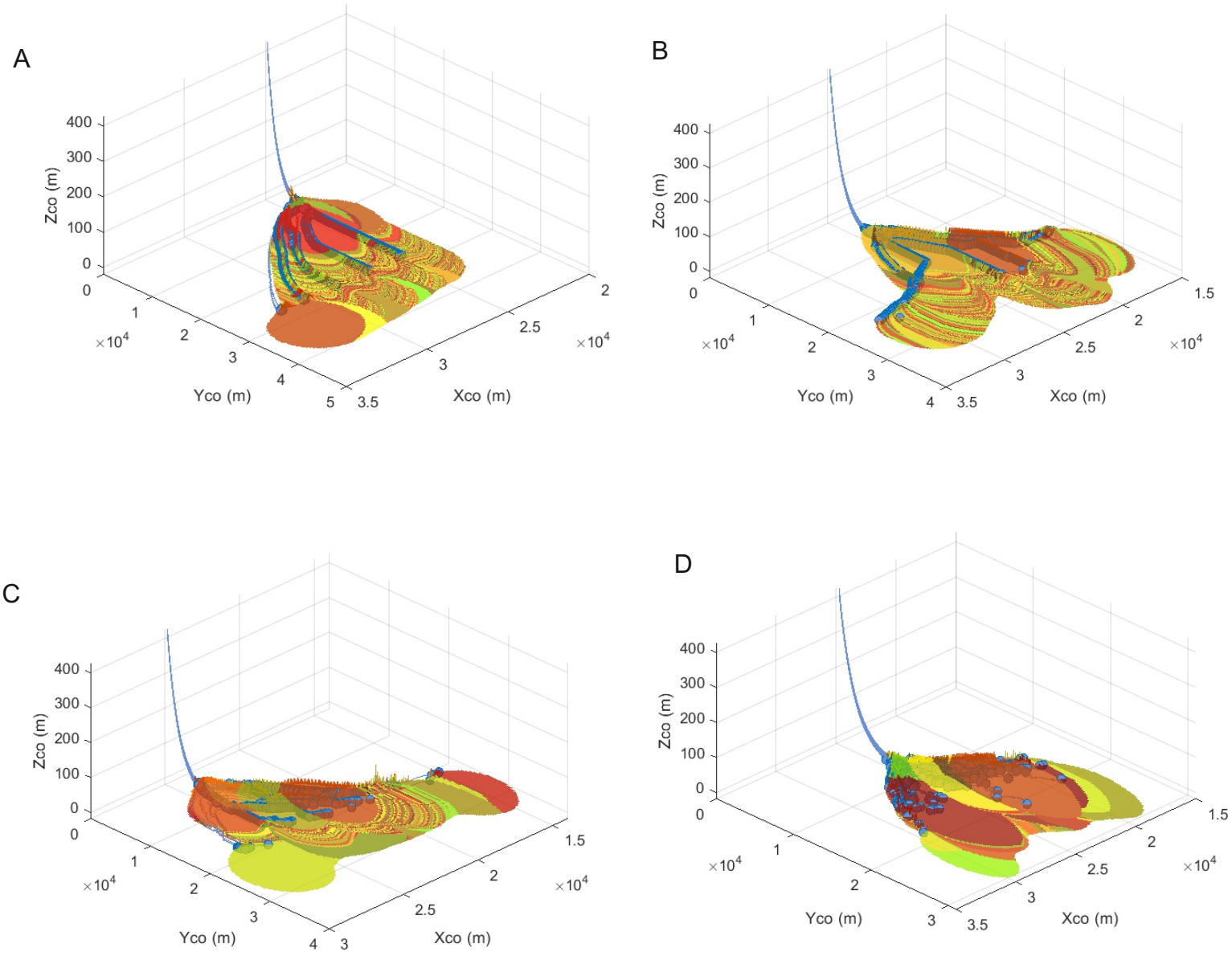

Figure

Click here to access/download;Figure;Figure 8 Lobyte3d strike sections.pdf

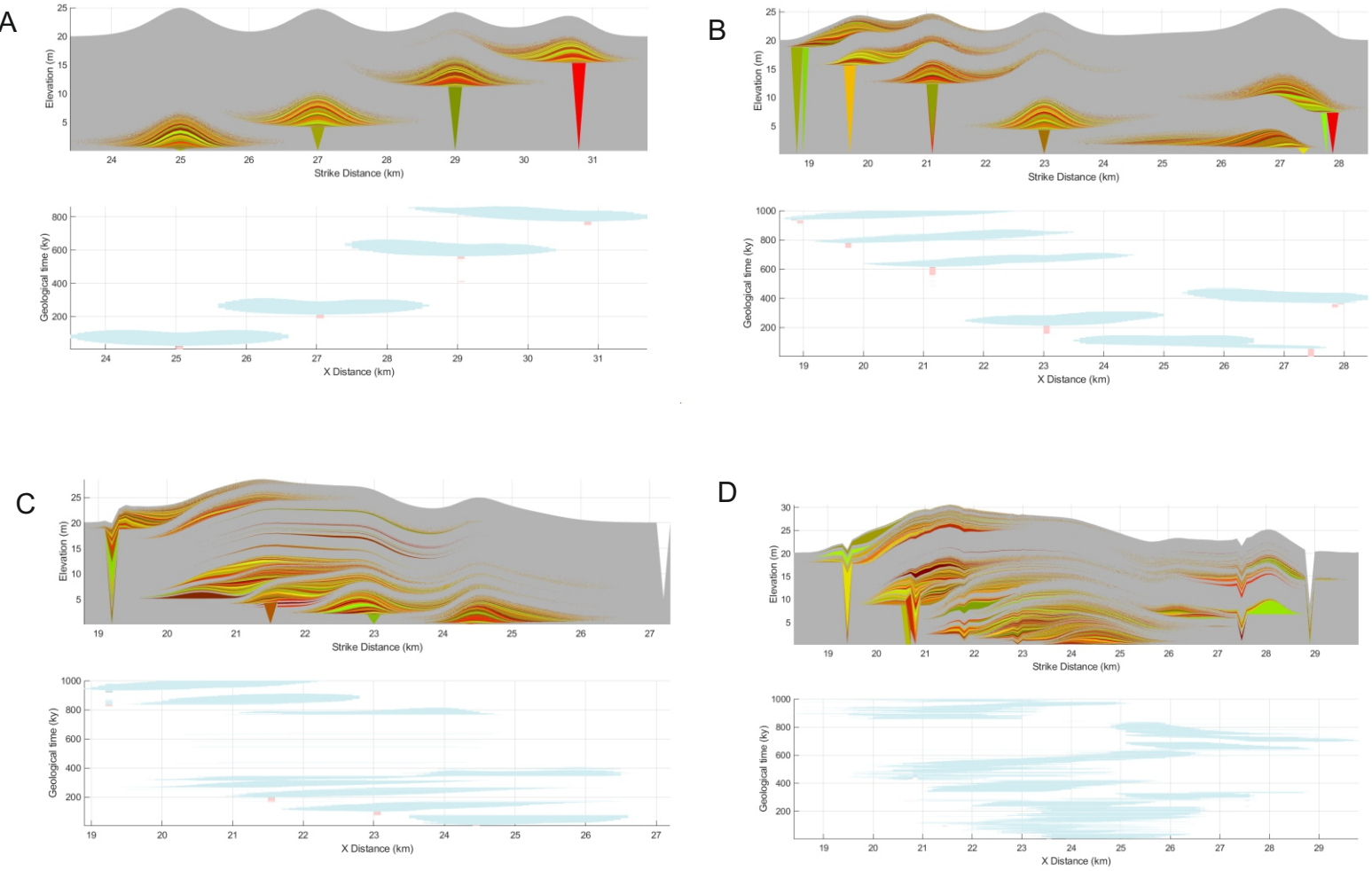

Figure

Click here to access/download;Figure;Figure 9 Lobyte3d flow centroids.pdf

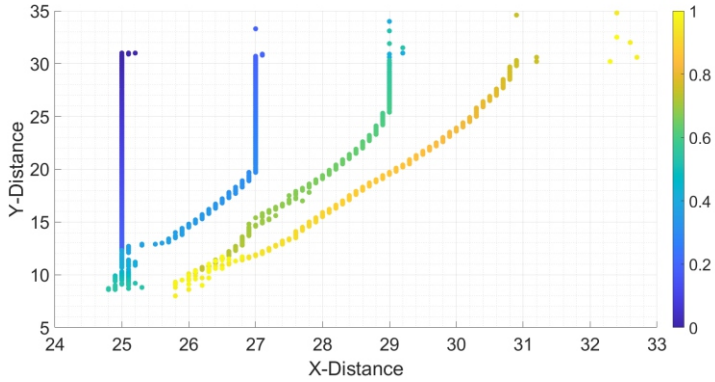

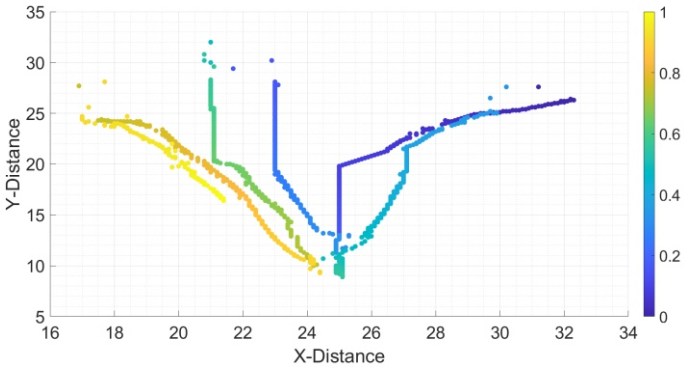

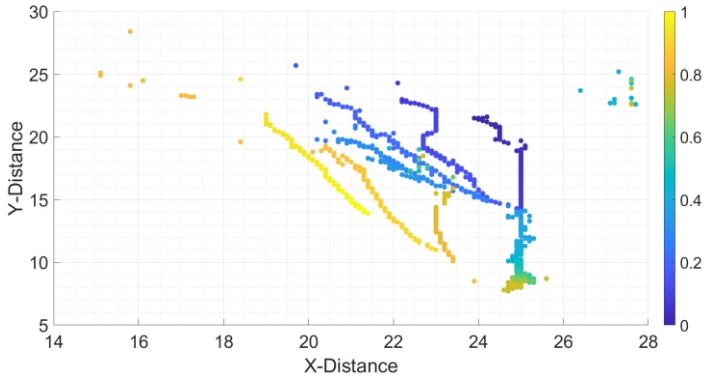

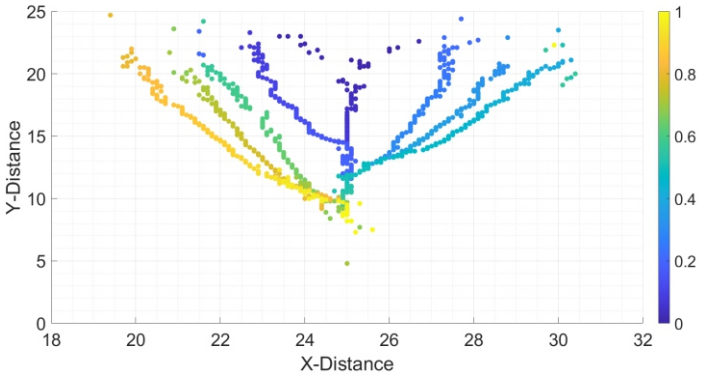

Figure

Click here to access/download;Figure;Figure 10 cluster and hierarchy metric lobyte plots.pdf

A.

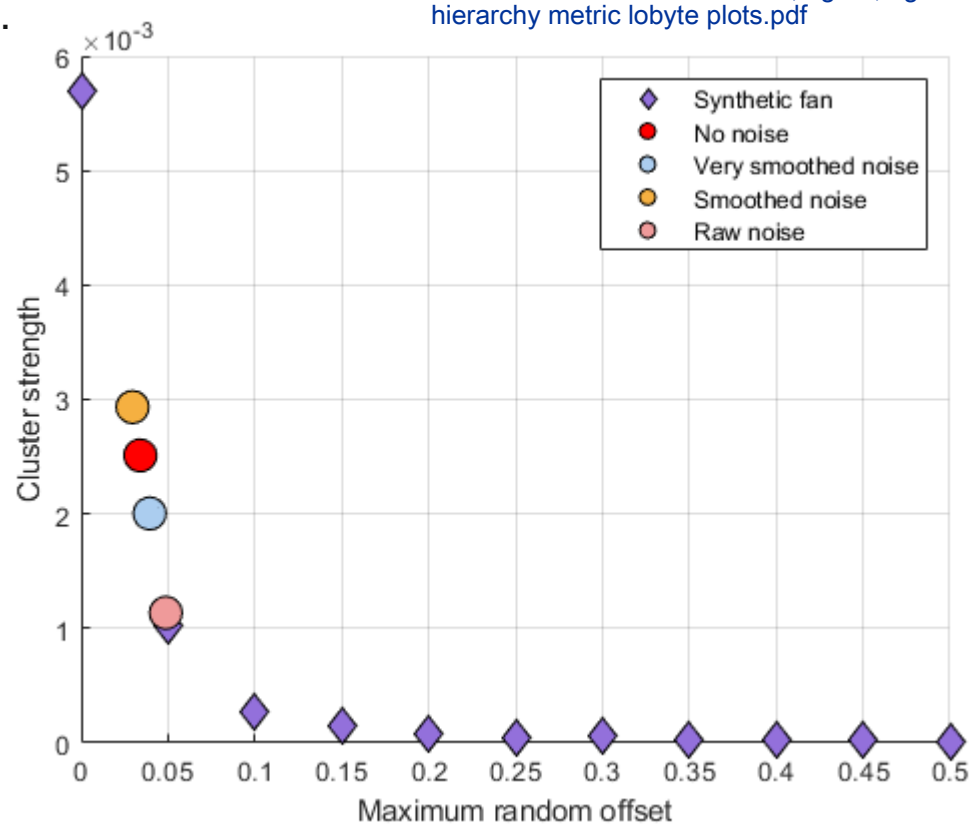

B.